Hydrology and Earth System Sciences, 4(4), *565–580* (2000) © EGS

Hydrology & Earth System Sciences

Radar hydrometeorology using a vertically pointing radar

I.D. Cluckie[1], R.J. Griffith[1], A. Lane[1] and K.A. Tilford[2]

[1]Water and Environmental Management Research Centre, Department of Civil Engineering, University of Bristol, Lunsford House, Cantocks Close, Bristol, BS8 1UP, UK
[2]Telford Research Institute, Department of Civil and Environmental Engineering, University of Salford, Manchester, M5 4WT
e-mail for corresponding author: i.d.cluckie@bristol.ac.uk

Abstract

A Vertically Pointing Radar (VPR) has been commissioned and deployed at a number of sites in southern England, to investigate numerically spatial and temporal variations in the vertical reflectivity profile (Z_{vp}); particularly those associated with the intersection by the radar beam of a melting layer – the bright band. Comparisons with data from other instrumentation, notably with the S-band research radar at Chilbolton, but also with disdrometer data and rainfall measurements from a number of sophisticated rain gauges, show that VPR scans of the atmosphere provide detailed and reliable quantitative measurements of the Z_{vp}. Analysis of a three year archive of Z_{vp} data for Manchester has shown a bright band to be present in over 80% of rainfall events, highlighting the extent of the problem of bright band errors in scanning weather radar data. The primary characteristics of the bright band such as the height and magnitude (in dBZ) of the top, bottom and peak are identified objectively from VPR Z_{vp} data by an automatic bright band recognition algorithm. It is envisaged that this approach could form the basis of an objective, automatic real time correction procedure for scanning weather radars.

Keywords: Vertically Pointing Radar, weather radar, hydrometeorology, bright-band, melting-layer, vertical radar reflectivity

Introduction

The primary objective of this research project was to commission and then deploy a mobile Vertically Pointing Radar (VPR) to study the hydrometeorology of rainfall systems and investigate the nature and extent of errors which can be introduced into scanning weather radar rainfall estimates by inhomogeneities in the vertical reflectivity profile (Z_{vp}). Of particular significance are bright band errors resulting from the intersection of the melting layer by the radar beam. Attempts to explain the existence of the layer of enhanced reflectivity on a radar image (the bright band) have been numerous since it was first observed on wartime radar scans in the 1940s. Some of the more notable studies include Byers and Coons (1947), Cunningham (1947), Austin and Bemis (1950), Battan (1973) and Battan and Bohren (1982). Stewart *et al.* (1984) related to radar measurements, the thermodynamic and microphysical changes through the melting layer in stratiform clouds and thereby inferred the dominant precipitation processes.

With decreasing height, the sequence of inferred precipitation processes may be summarised as follows (see Stewart *et al.*, 1984). Although there is a good agreement on the significance of these processes in the melting layer, other work is referred to where necessary:

1. A peak in ice particle concentration around the −5°C level with ice particle multiplication (by rime splintering) the dominant process.
2. Towards and within the 0°C layer, as the temperature increases, aggregation of ice particles becomes the most important activity; this is shown by an increase in particle size and an accompanying decrease in particle concentration.
3. The particles melt as they fall through the melting layer, the smallest ones completing melt-out first. It is the increased dielectric constant and backscattering effects of the largest aggregates, which are only partially melted on reaching the base of the isothermal layer, that causes the maximum radar reflectivity (bright band) to appear a few 100 m below (Willis and Heymsfield, 1989).
4. Below the bright band, there is an increase in the fall speed of particles from around 1–2 ms^{-1} in the region above the bright band to about 5–6 ms^{-1} below as the drops collapse upon melting (similar measurements have been made by Lhermitte and Atlas (1963)). These fall speed and shape changes result in a decrease in particle concentration, causing the radar reflectivity to be lower in this region.
5. In the rain area below the bright band, a raindrop size spectrum evolves as the concentration of large drops falls and that of the smaller ones increases. These observations are consistent with collision-induced breakup i.e. drops of differing fall speeds coalesce and grow to reach a

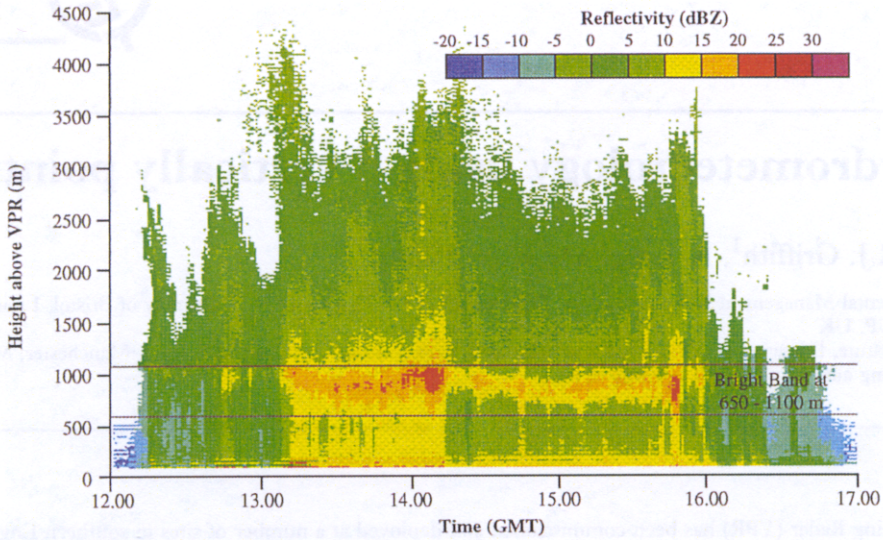

Fig. 1. *Height time image from a VPR located at Salford on 14 April, 1992 showing a typical bright band.*

limiting size when the drops break up (Klaassen, 1988; Steiner and Waldvogel, 1989).

An example bright band, as measured by a VPR, is shown in Fig. 1. Interception of the bright band can cause overestimates of up to a factor of 5 (Joss and Waldvogel, 1990), but this depends on how much of the beam is filled by the bright band. A typical thickness, observed with the VPR, is of the order of 300 m. Problems of overestimation will therefore be most severe close to scanning radar, when the small vertical beam depth is able to resolve the bright band. At medium range, enhancements caused by the bright band may compensate for the reduced reflectivity typically measured at this range because the beam may be a few kilometres above the ground, and at longer ranges underestimation of precipitation estimates dominates.

Variability in Z_{vp} is limited not just to the region around the melting layer. Because the height of the beam increases with range, particles with different reflective properties, shapes, sizes and fall speeds are illuminated. Above the bright band, in the region of snow/ice, which has a lesser absorption coefficient, reflectivity profiles tend to show a sharp decrease with height, changing by up to a factor of 4 in measured rain per kilometre (Joss and Waldvogel, 1990). Also, one of the main problems of radar rainfall measurements at long range (>100 km) is that low level precipitation can be missed altogether. This problem is exacerbated when low-level enhancement occurs below the beam. Such a situation is critical when radar data are used within a flood warning system for example. Low level enhancement occurs mainly over hilly terrain. The main causes are auto conversion, whereby cloud is formed due to its ascent up and over the hill, seeding by raindrops from high level cloud into terrain-induced low level cloud or by raindrops produced from triggered convection due to forced uplift over the hills during unstable conditions.

Numerous identification and correction methods have already been proposed, based upon information of Z_{vp}, such as Joss and Waldvogel (1970), Harrold and Kitchinman (1975), Smith (1986), Klassen (1988), Gray (1991), Gray and Uddstrom (1997), Koistinen (1992), Hardaker (1993), Hardaker *et al.* (1995), Andrieu and Creutin (1995), Kitchen *et al.* (1994). With the exception of Gray and Uddstrom (1997), who base Z_{vp} construction on 10 levels of scanning radar data separated by 0.25 km, none of these schemes represents Z_{vp} in great detail and/or is based directly on measured profiles. A detailed analysis of very high resolution Z_{vp} data has therefore been conducted to further understanding of bright band characteristics and support the development of numerical models to correct for errors in quantitative precipitation estimates derived from scanning weather radars.

This paper describes the instrumentation used during the project and the locations at which the equipment was deployed. It then presents a data intercomparison study in which measurements of ground-based rain gauges and a disdrometer, and from the experimental S-band Chilbolton radar are compared with VPR Z_{vp} data. The utilisation of VPR Z_{vp} data for the objective identification and quantification of bright bands and Z_{vp} variability are discussed. Finally, an analysis of a long-term archive of VPR Z_{vp} observed at Manchester is presented.

Experimental sites

Sites at Middle Wallop, Boscombe Down and Alhampton, in South West England, were selected (see Fig. 2). Radio clearance was granted for all sites in February, 1994.

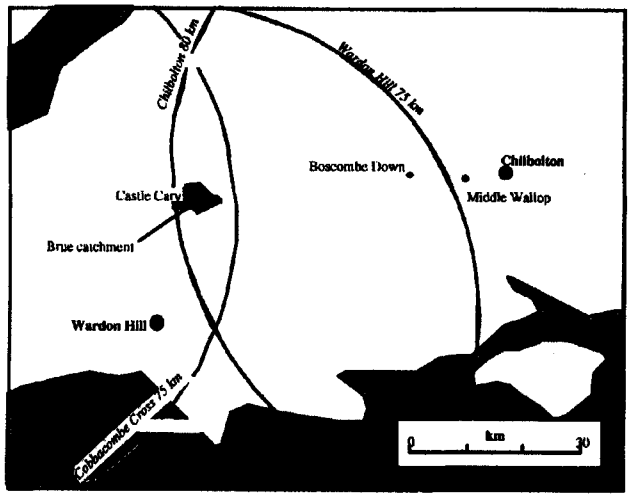

Fig. 2. *HYREX radar sites.*

The two more easterly sites (Middle Wallop and Boscombe Down) were chosen for their proximity to the Chilbolton radar site to enable direct comparison with the highest resolution data from the radar. Both sites were located within Ministry of Defence bases which provided the high level of security required for unmanned operation of the equipment. A VPR was operated at Middle Wallop from May–November, 1995 whilst Boscombe Down was operational from April–August, 1995.

The third site at Alhampton near Castle Cary provided an opportunity to obtain data over the River Brue catchment. The site was also located within one of the two designated dense rain gauge networks (Moore *et al.*, 2000) and within the nominal quantitative (75 km) range of the Wardon Hill and Cobbacombe Cross Meteorological Office network weather radars. Site preparation prior to deployment included the construction of a secure compound and the provision of mains power. A VPR operated at Alhampton from August–December, 1995.

Instrumentation specifications

The instrumentation operated by the University of Salford team included two mobile VPRs, two transportable Automatic Weather Stations (AWS), two high intensity drop counting (Hydra) rain gauges and a disdrometer[1]. The standard procedure was to operate a mobile VPR together with an AWS and Hydra gauge. Details of the instrumentation deployed are provided in the following sections.

VERTICALLY POINTING RADARS

The final installation and testing in the VPR trailer system took place during April, 1994. The principal technical specifications are given in Fig. 3 which also shows the VPR. The devices operate at a nominal frequency of 9380–9440 MHz at a 3 cm wavelength (X band) and provide 7.5 m reflectivity data (this setting was used throughout the experiment) through a vertical column of the troposphere at a maximum temporal resolution of 2 seconds. Additional specification and operational details may be found in Tilford *et al.* (1995). Reflectivity is calculated from the standard radar equation (Battan, 1973). At frequencies of X and C, questions arise as to the validity of this equation because of the assumption of Rayleigh scattering. However, the investigation by Wexler and Atlas (1963) showed that results using the Rayleigh approximation do not differ appreciably from results using deviations from this approximation at wavelengths of 3 cm or more. Therefore, the assumption of Rayleigh scatter is assumed valid at the X-band frequencies used in this project. They employed the Mie theory of scatter and Mie backscattering cross sections (σ) computed by Herman *et al.* (1961) and calculated $\Sigma\sigma$ for rainfall rates between 0.01 and 100 mm hr^{-1} and for wavelengths between 0.62 and 10 cm.

AUTOMATIC WEATHER STATION

The AWS is industry standard instrumentation with sensors for the measurement of the standard range of meteorological variables: rainfall, wet and dry bulb temperatures, wind speed and direction, ambient atmospheric pressure, air humidity and incoming and net solar radiation. The rain gauge is a tipping bucket device with a bucket size of 0.1 mm depth equivalent. The AWS logger sampled the meteorological variables at 10 second intervals with subsequent averaging (or accumulation in the case of rainfall depth) over a two minute period prior to data logging.

HYDRA GAUGE

A second rain gauge known as a Hydra gauge was used throughout the study. The Hydra sensor, developed at the Atmospheric Physics Group at the University of Auckland, New Zealand (Stow, 1993) is a high resolution, solid-state device which operates by channelling rain water via a collection funnel through a 'dropper' which produces a stream of constant size droplets. These droplets pass between two parallel wires causing a circuit closure which enables the drops to be counted prior to logging on an EPROM unit. The number of drops within a pre-defined period (maximum resolution 15 seconds) can then be converted to a rainfall intensity. A nominal calibration of 160 drops mm^{-1} enables the Hydra gauge to measure rainfall rates of up to 200 mm hr^{-1}.

[1]In association with the Rutherford Appleton Laboratory.

General	
Radar Type	*Racal Marine Navigation Transmitter*
Frequency	*9380 - 9440MHz*
Wavelength	*approx. 3cm (X Band)*
Antenna	
Antenna type	*Parabolic reflector*
Antenna diameter	*1.2m*
Beam	
Beam elevation	*Vertically pointing*
Beamwidth	*1.8° (between half-power points)*
Power	
Mean power to antenna	*12 dBW*
Peak power to antenna	*44 dBW (25 kW)*
Relative gain of antenna	*38 dB*
Radiative	
Pulse recurrence frequency	*1300 / 650 Hz*
Pulse width	*0.05 / 0.25 / 1.0μs*
Polarisation	*Linear*
Observation	
Minimum height	*100 m (above site)*
Vertical resolution	*7.5 m max.*
Temporal resolution	*2 s max. (1200 pulses averaged)*

Fig. 3. *The HYREX VPR and principal technical specification.*

DISDROMETER

An RD-69 'Distromet' disdrometer (Joss and Waldvogel, 1970) was deployed at Boscombe Down. The transducer unit generates electrical pulses by converting the momentum of the rain drops as they strike a styrofoam cone. Pulse amplitude is proportional to drop momentum enabling the size (diameter) of each droplet to be estimated. Unwanted signals such as acoustic noise are filtered by signal processing. Processed data are in the form of the number of drops averaged over one minute for twenty drop size classes within a range 0.3–5.0 mm. A computer was connected to the processor to receive and store the data. The disdrometer was placed in a shallow well so that the top of the device was flush with the ground surface to minimise intrusion into the local wind field which is a potential source of acoustic noise.

CHILBOLTON RADAR

The experimental Chilbolton radar (Goddard *et al.*, 1994) is one of the world's largest steerable meteorological radars as it can perform 360° plan-position indicator (PPI) scans and range-height indicator (RHI) scans from 0°–90°. The main radar operates at S-band (10 cm wavelength) and has a beam width of 0.25°. The antenna diameter is 25 metres.

The maximum resolution of the radar data along the radial (minimum bin length) is 300 m although the narrow beam width results in a bin width of just 44 m at a range of 10 km. For the purposes of this project, a scan regime was developed in conjunction with the Rutherford Appleton Laboratory: RHI scans were made along the bearings of the three VPR sites (268°, 270°, 272°) followed by a 90° sector scan in PPI mode at 1° and 5° beam elevations centred around a 270° bearing.

RAPID RESPONSE GAUGES

Data from two rapid response rain gauges operated by Rutherford Appleton Laboratory and capable of measuring rainfall intensities at 10 second intervals were also used in the study for data verification purposes. Both devices were located at the Boscombe Down site (as part of a separate experiment) at a distance of between 500–1000 m from the VPR and associated instrumentation. Further information on these gauges is provided in the paper by Illingworth *et al.* (2000).

RADIOSONDES

A Meteorological Office site at Larkhill used for the release of radiosondes is approximately 10 km due west of the Boscombe Down site. Regular quarter day releases were made at 00.00, 06.00, 12.00 and 18.00 GMT. The sonde data have been analysed primarily for information on the vertical temperature structure of the atmosphere, wind speed and direction.

Data quality control

Discussion of the data analysis will focus on two rainfall events simultaneously observed by VPRs deployed at Boscombe Down and Middle Wallop. All additional instrumentation (i.e. that deployed with the VPR) was also operational during these events allowing the analysis of data for events with different meteorological structures and rainfall intensities. The analysis provided the opportunity to establish a measure of confidence in the observed data by comparing reflectivity values calculated from the observed drop size distribution at the ground with VPR reflectivity data.

The event of 11 May, 1995 lasted for approximately 10 hours and was characterised by weak, widespread rainfall associated with a cold front. Total rainfall accumulations were less than 2.0 mm. The second event, occurring on 16 May, again lasting for approximately 10 hours, was associated with an occluded front that moved in a northerly direction over England. The drop in surface temperature throughout the event suggests a cold occlusion. The rainfall exhibited less temporal variation than the 11 May event and the total event rainfall accumulation was 5.2 mm.

RAIN GAUGE AND DISDROMETER COMPARISONS

The following analysis was performed to assess the extent of any equipment errors during the observation periods and the level of agreement in rainfall intensity and depths between the respective data sets.

The combination plots of intensity time series and accumulated rainfall hyetographs (Figs. 4a, 4b) show close agreement between the accumulated totals computed from the disdrometer drop size spectra and tipping bucket gauges for both events. The Hydra sensor overestimates rainfall for both events, most significantly on the 16 May, due to a minor error in the calibration setting on the gauge. This was subsequently corrected by a simple calibration test and data reconstitution. Although a perfect match in totals is rarely obtained (nor expected), the similarity of the observations indicate that event cumulated depths, computed as the average of all the observed totals can be regarded as a true estimate of total event rainfall.

The two Rutherford Appleton Laboratory drop counting gauges provide independent verification of event rainfall intensities and depths. The gauges are at different sites between 500 m and 1000 m from the disdrometer, Hydra gauge and tipping bucket gauge: some inter-instrument variation due to small scale spatial variability in the rainfall is therefore expected. The rainfall intensity time series and accumulated totals for both events (Figs. 4c, 4d) show similar trends particularly on the 16 May due to the constant, widespread nature of the rainfall.

The rainfall intensity time series reveal an inability of the Hydra sensor to resolve light rain intensities such as occurred on 11 May (mean rain rate, 0.13 mm hr^{-1}). In such circumstances, the Hydra gauge time series contains many null values. This is reflected in the Hydra gauge/disdrometer event data correlation coefficient of $r = 0.39$ and is also apparent in the autocorrelation functions (ACF) of the rainfall intensity time series of each device (Figs. 4a, 4b) with significant differences between the ACF of the Hydra gauge and disdrometer: the lower autocorrelations of the former arise from the null values in the data set. It is interesting to note that the ACF for the RAL gauges (Figs. 4c, 4d) display the same characteristics as the Hydra gauge but with even lower autocorrelations. These results indicate a failing of drop counting rain gauges to resolve low intensity rainfall, most likely due to the evaporation of the rain water droplets off the gauge funnel. In contrast, the rainfall intensity observations for the more intense event of 16 May (mean rainfall intensity, 0.48 mm hr^{-1}) exhibit a significantly higher correlation $r = 0.92$ and the Hydra gauge and disdrometer ACF are almost identical.

Other factors which may also account partially for the observed variations in the data include differences in device calibration and sensitivity. The disdrometer, for example, is not very sensitive to drops below 0.3 mm diameter; this will affect the results measured during the weak rainfall on the 11 May in particular. Also, the instrument site has a bearing on overall rainfall catch. The tipping bucket gauge top was sited 0.5 m above the ground, the Hydra sensor was mounted on a pole 1.5 m above ground level and the disdrometer was sited flush with the ground surface. The terrain of the site was also uneven, the rain gauges being on slightly higher ground than the disdrometer. Localised sorting of raindrops due to wind turbulence near the surface will also introduce variations into the measurements.

VPR AND DISDROMETER COMPARISONS

This section compares the quality controlled disdrometer data with reflectivity measurements from the VPR. For the purposes of this comparison, mean reflectivity values computed from bins 34–40 (255–300 m) of the VPR Z_{vp} were used. Previous analysis of VPR Z_{vp} data by Tilford *et al.* (1994) showed this approach overcame potential problems associated with ground echoes. Reflectivity time series, scattergrams and ACF for the VPR and disdrometer data for the two case study events are shown in Fig. 5 (Fig. 5a, 11 May: Fig. 5b, 16 May).

The reflectivity time series for the two events for each device exhibit a high degree of correlation ($r = 0.89$ and $r = 0.96$ respectively) although a significant systematic error is present. A regression analysis of the two data sets was performed, and the least squares best fit of the data shown in the scattergrams give relationships of the form:

$$\text{11 May: } y = 0.90\,x + 8.57 \quad (1)$$

$$\text{16 May: } y = 0.97\,x + 7.23 \quad (2)$$

where for the purposes of the regression, the disdrometer data were treated as the independent variable.

The similarity in the gradients indicate that the observed differences in reflectivity are largely independent of rainfall intensity. If the slope is assumed to be 1.0 for both events and the VPR data are recalculated, the average systematic difference calculated over the two events is 7.9 dBZ. It is thought that this is attributable to VPR overestimation given the observations presented earlier. A systematic difference of 7.9 dBZ over a range of reflectivities from −20 to 40 dBZ would cause rainfall rates to be much greater at values near to 40 dBZ. If rainfall rates are the only usable or retrievable

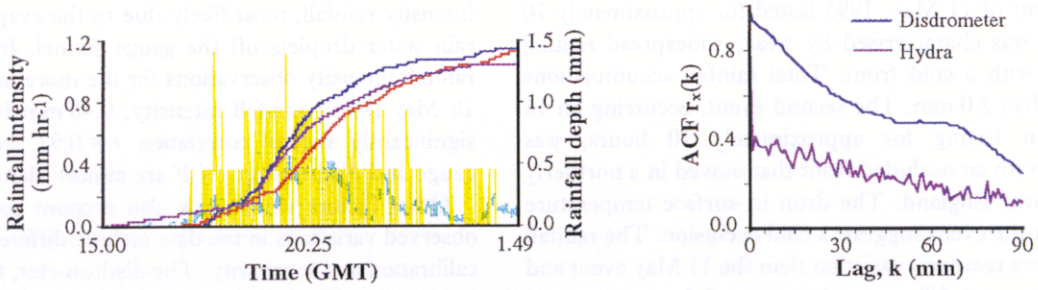

(a). 11th May: Disdrometer, Hydra gauge, tipping bucket gauge

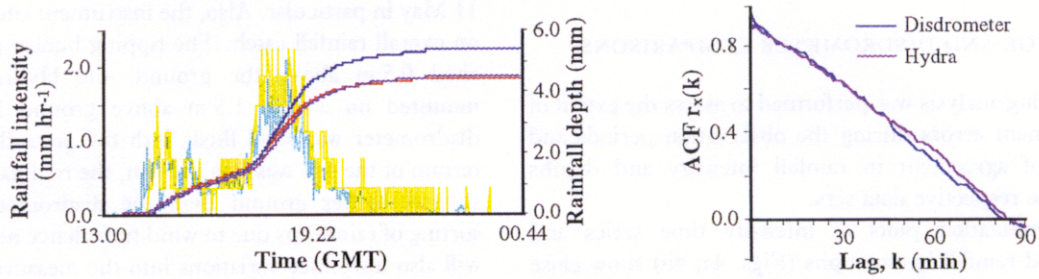

(b). 16th May: Disdrometer, Hydra gauge, tipping bucket gauge

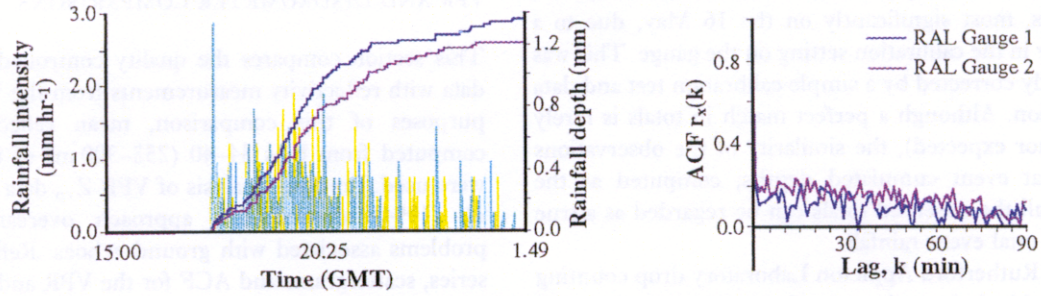

(c). 11th May: RAL gauges

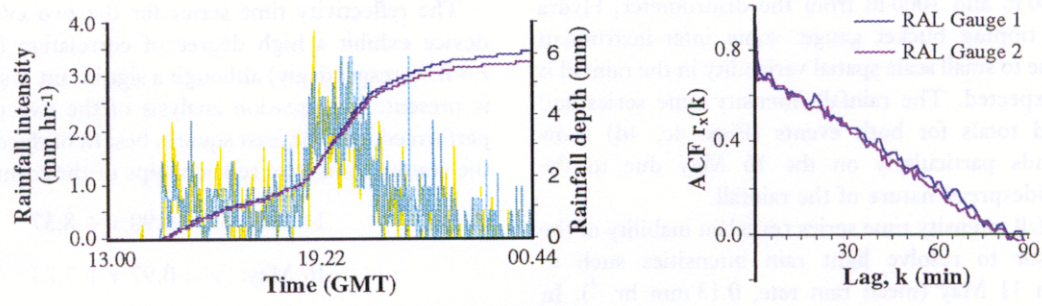

(d). 16th May: RAL gauges

Key for a and b

- Disdrometer rainfall intensity
- HYDRA rainfall intensity
- HYDRA accumulated depth
- Tipping bucket accumulated depth
- Disdrometer accumulated depth

Key for c and d

- RAL Gauge 1 rainfall intensity
- RAL Gauge 2 rainfall intensity
- RAL Gauge 1 accumulated depth
- RAL Gauge 2 accumulated depth

Fig. 4. *Rainfall intensity time series, accumulated rainfall and autocorrelation functions as recorded by a variety of instrumentation for 11 and 16 May, 1995 at Boscombe Down.*

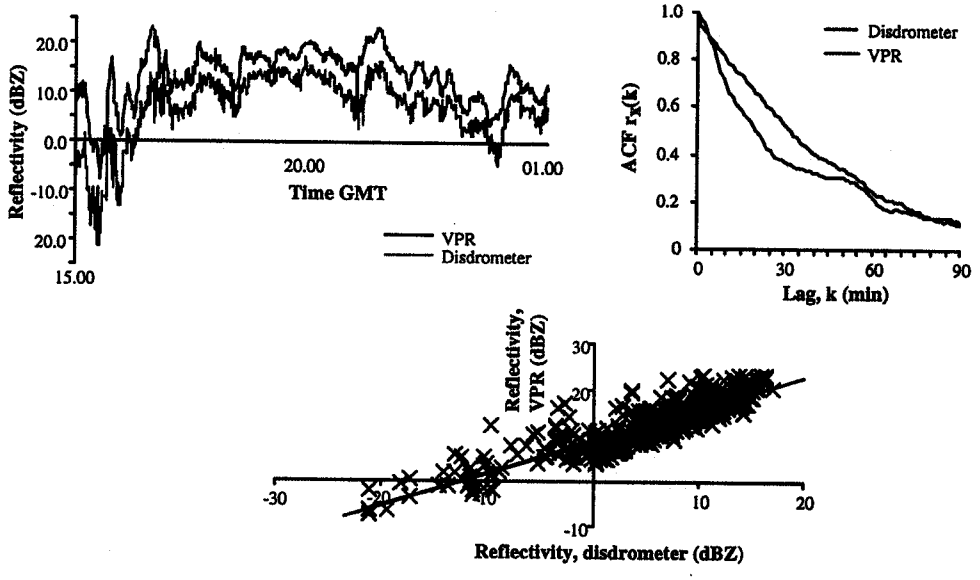

(a). 11th May

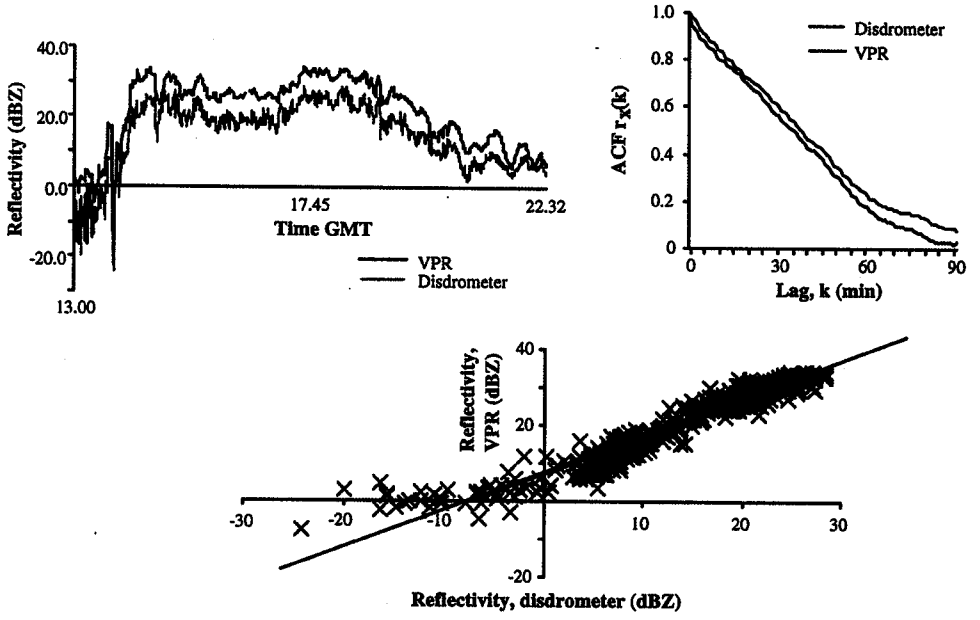

(b). 16th May

Fig. 5. *Reflectivity time series, autocorrelation functions and reflectivity scattergrams for VPR and disdrometer data for 11 and 16 May, 1995 at Boscombe Down.*

input available for hydrological modelling (i.e. no raw radar data are available) a systematic difference of this magnitude would be problematic at the higher rainfall rates.

The event ACF for the VPR and disdrometer reflectivity time series are similar and exhibit a high degree of autocorrelation at small lags. Short-term correlations mean that an observation above the mean tends to be followed by one or more further observations above the mean (and similarly for observations below the mean) and this pattern is consistent with rainfall made up of precipitation cores.

VPR HEIGHT-TIME IMAGE DATA AND DISDROMETER DROP SIZE DISTRIBUTIONS

Figures 6 and 7 show the VPR height-time image (HTI)

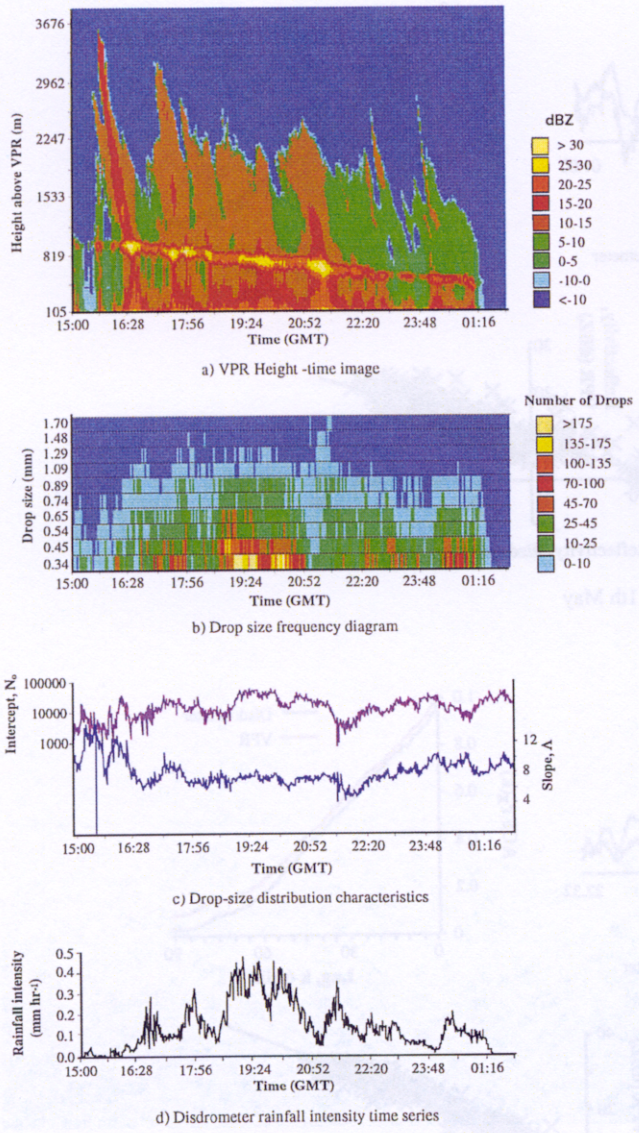

Fig. 6. *VPR, disdrometer and HYDRA gauge data for 11 May, 1995 at Boscombe Down.*

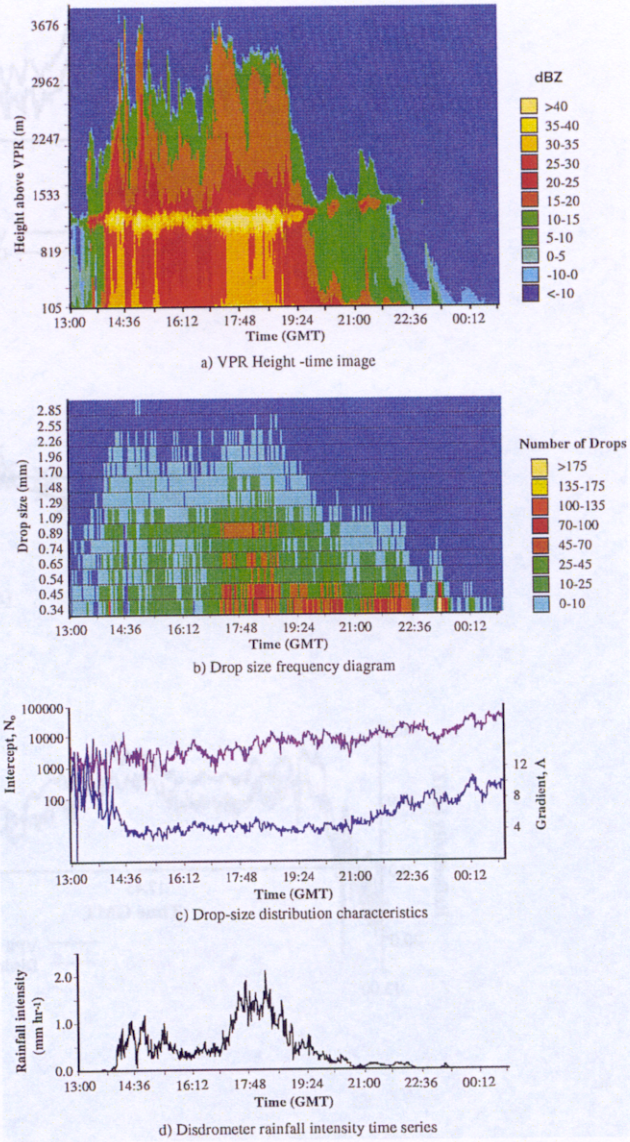

Fig. 7. *VPR, disdrometer and HYDRA gauge data for 16 May, 1995 at Boscombe Down.*

(Figs. 6a, 7a), disdrometer drop-size distributions (DSD) (Figs. 6b, 7b), plots of the intercept (N_0) and slope (Λ) values calculated from the disdrometer DSD using the exponential relationship given in Eqn. 3 (Figs. 6c, 7c) and the rainfall rate calculated from the disdrometer (Figs. 6d, 7d) for the case study events.

Precipitation trails and precipitation cores

The event HTIs (Figs. 6a, 7a) particularly for 11 May display snow trails above the bright band. Reflectivities increase downward towards the bright band presumably due to aggregation. The rain below the intersection of the trails is more intense there than elsewhere due to the melting snow.

Similar reflectivity patterns have been observed by other researchers. Marshall (1953) and other investigators at the time observed snow trails in HTI and RHI imagery. Plank *et al.* (1955) concluded that such trails play an important role in the development of stratiform precipitation. On the other hand, Carbone and Bohne (1975) found the latent heat of melting near the 0°C isotherm could generate instability and consequently a weak convective layer.

In accordance with these previous observations, analysis of radiosonde data for the two events (11 and 16 May) reveals a layer of conditionally unstable air immediately above the bright band. On 16 May, there was a temperature inversion at an altitude of approximately 2 km to 3 km which would cap convection unless the rising parcels had sufficient momentum to continue upwards (see Figs. 8, 9).

Drop size distributions

The distributions observed in raindrop sizes are caused by

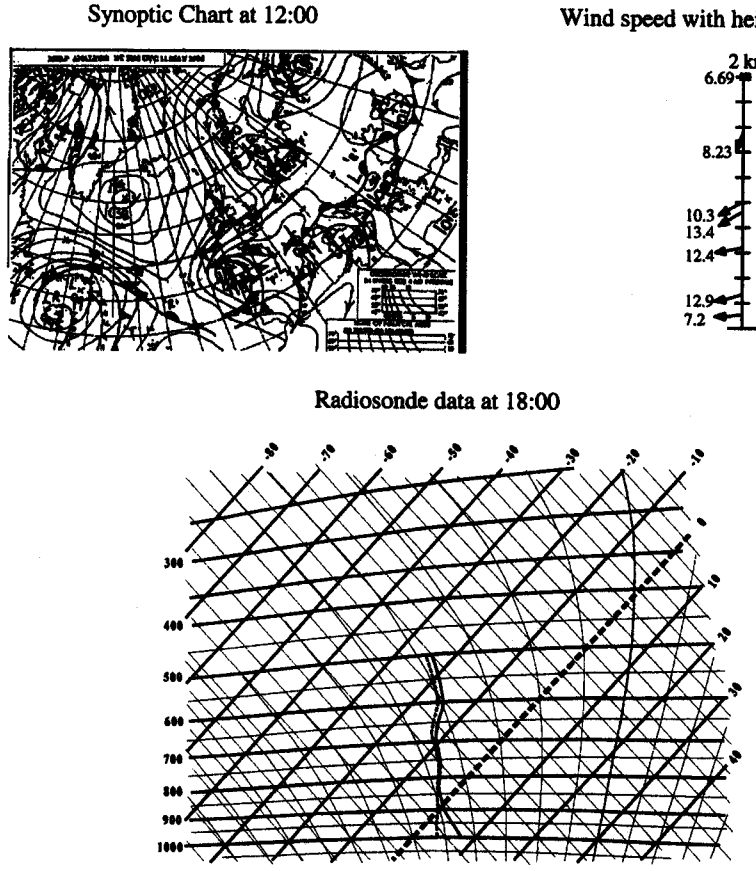

Fig. 8. *Synoptic charts, Larkhill radiosonde data (generated from numerical data) and wind speeds (ms^{-1}) and direction (up is 0° north and down is 180° south) up to 2 km altitude for the 11 May.*

the process of raindrop formation. Snow particles of many sizes melt and hence form raindrops of different sizes. As these raindrops fall they grow chiefly by sweeping up other smaller drops. Also, raindrops disintegrate once they reach a maximum size, which depends on the aerodynamically induced circulation of water in the drop, or, if they collide with other drops. This break-up produces more smaller drops which themselves contribute to droplet growth and hence the break-up process again. DSDs express the number of drops per unit size interval (usually diameter) per unit volume of space. The typical form of a distribution, which is variable in time and space, is indicated by a rapid decrease in drop concentration with increasing drop size. Also, they generally show a systematic variation with rainfall intensity, as the relative number of large drops tends to increase with rainfall rate, Rogers and Yau (1989).

DSDs have been examined for use in different synoptic situations such as reported in Houze *et al.* (1979), Du Toit (1967), Bringi and Chandrasekar (1987) and Zawadski *et al.* (1994). There is also a general distribution which incorporates all previous DSDs (Sempere Torres *et al.*, 1994). One of the most referenced DSDs is that of Marshall and Palmer (1948) (MP) who fitted a negative-exponential curve to their measurements. The parameters N_0 and Λ of the DSD measured by the disdrometer are derived by fitting the MP distribution, which is expressed as,

$$N_D = N_0 \exp(-\Lambda D) \quad (3)$$

where $N_D\ \delta D$ is the number of drops of diameters between D and $D + \delta D$ in a unit volume of space, N_0 is the value of N_D for $D = 0$, and:

$$\Lambda = 41R^{-0.21} \quad (4)$$

is the slope of the exponential curve where R is the rain intensity (mm hr^{-1}) computed from reflectivity (Z) and liquid water content (W) values derived directly from the disdrometer DSD (Figs. 6b, 7b).

Figures 6c and 7c show N_0 and Λ time series for each event. The high positive correlation coefficients: (11 May, $r = 0.6$; 16 May, $r = 0.86$) especially for the latter, indicate that N_0 and Λ are directly related and that Λ increases with N_0 (increase in the number of small drops) and vice-versa.

The precipitation trails observed in the event HTI for 11 May (Fig. 6a) cause an enhancement of the bright band and a subsequent enhancement of rainfall rates which are observed at the ground. The event drop size frequency distribution (Fig. 6b) shows that until 21.00 the drop-size

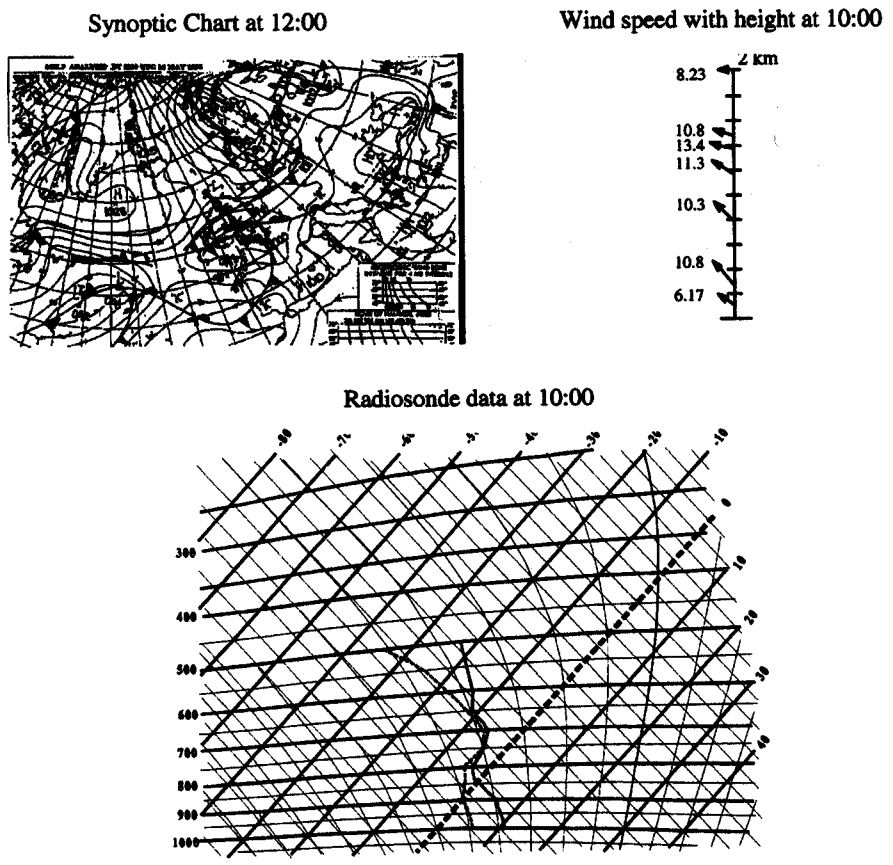

Fig. 9. *Synoptic charts, Larkhill radiosonde data (generated from numerical data) and wind speeds (ms^{-1}) and direction (up is 0° north and down is 180° south) up to 2 km altitude for the 16 May.*

distribution is dominated by large numbers of small drops, particularly between 19.00 and 21.00 – also the time of heaviest rainfall. After 21.00, the number of small raindrops suddenly decreases but larger drops continue to be present and cause a maximum peak in the radar VPR reflectivity. This illustrates the dominance that a small number of large drops can have in the calculation of Z. However, the rainfall intensity (Fig. 6d) actually falls from the previous period.

The drop size frequency distribution for 16 May (Fig. 7b) shows the presence of larger drops than for 11 May (maximum diameter 2.85 mm as opposed to 1.7 mm on 11 May). Overall there are fewer small drops. The presence of triangular shapes in the drop size frequency distribution, a phenomenon noticed by Hobbs and Locatelli (1978) can be attributed to the combination of larger drops and greater numbers of drops occurring in the centre of precipitation cores. The steady increase in both N_0 and Λ through the event (Fig. 7c) suggests a gradual transition from larger to smaller drops.

There is further evidence of different radar reflectivities corresponding to the same rainfall rates at 15.00 and 19.24 (see Fig. 7a): the VPR reflectivity is 32 dBZ and 28 dBZ respectively but, at both times, the rainfall rate derived from the disdrometer (Fig. 7d) is 0.75 mm hr^{-1}.

On both days, the trends of N_0 and Λ are highly positively correlated. This suggests that the dominant factor in the fluctuation of rainfall rates is not due to the variation of raindrop sizes but due to increasing numbers of drops of the same size. If an assumption is made that for each sampling period of 1 minute, the disdrometer may fail to measure – (i) small drops due to inadequate sensitivity of and/or turbulence around the instrument; and (ii) less frequently occurring larger drops because of the size of the impacting surface – then gamma distributions with physically realistic values of m (between -2 and $+2$) (Ulbrich, 1983) can be formulated. When based upon event rainfall rates, the formulated distributions show the effect of synthetically generated drop numbers on the disdrometer reflectivity time series. This will help to highlight a possible theory for the disdrometer and VPR reflectivity discrepancy.

Figure 10 shows the disdrometer DSD computed from the mean drop numbers for each drop size bin through the whole event. The theoretical distributions computed using a MP exponential distribution (Eqns. 3, 4) and gamma distributions (Eqn. 5) for $m = -2$ and $m = 2$ are also shown. In all cases, the distributions are based on the average event rainfall rate derived from disdrometer data when drops were

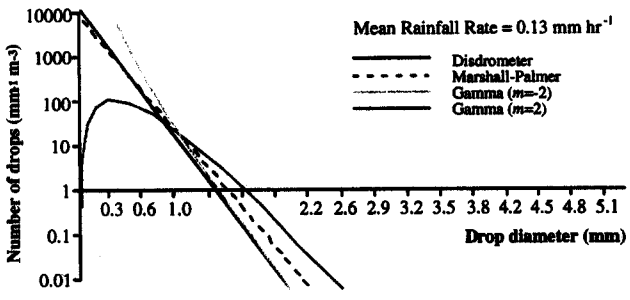

a). 11 May, 1995

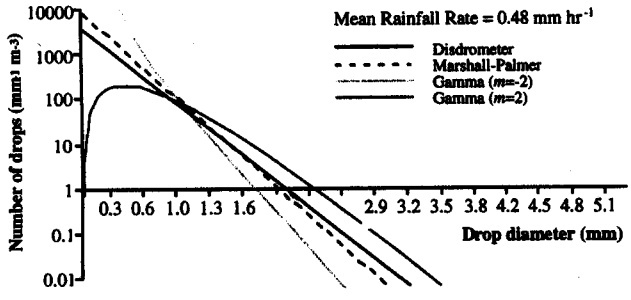

b). 16 May, 1995

Fig. 10. *Observed and theoretical drop size distributions.*

registered.

$$N_D = N_0 D^m \exp(-\Lambda D) \qquad (5)$$

The MP distribution is a special case of the gamma distribution when m = 0. Values of m = −2 to 2 were therefore chosen in an attempt to model DSDs that may be skewed to greater numbers of larger drops (m = −2), greater numbers of small drops (m = 2) or a more median value (m = 0).

Assuming an infinite drop diameter range and a gamma distribution with $m = -2$ to 2 respectively, each one minute disdrometer DSD is fitted by the gamma distribution. In each case, the value of m is chosen so that the distribution is a best-fit to the data whilst taking account of possible missed drops. The reflectivity can then be recalculated using actual event rainfall rates to estimate the likely effect on comparisons of disdrometer Z and VPR Z using:

$$Z = \frac{N_0 \Gamma(m+7)}{\Lambda^{m+7}} \qquad (6)$$

where Γ is the gamma function.

Ideally the integration should be carried out over a finite diameter range, but the difference between an assumption of a maximum drop diameter of 5 mm and infinity on the calculations is marginal, especially at such low rainfall rates.

The recalculation of Z with the enhanced drop size distributions was carried out for the two events. Overall, the

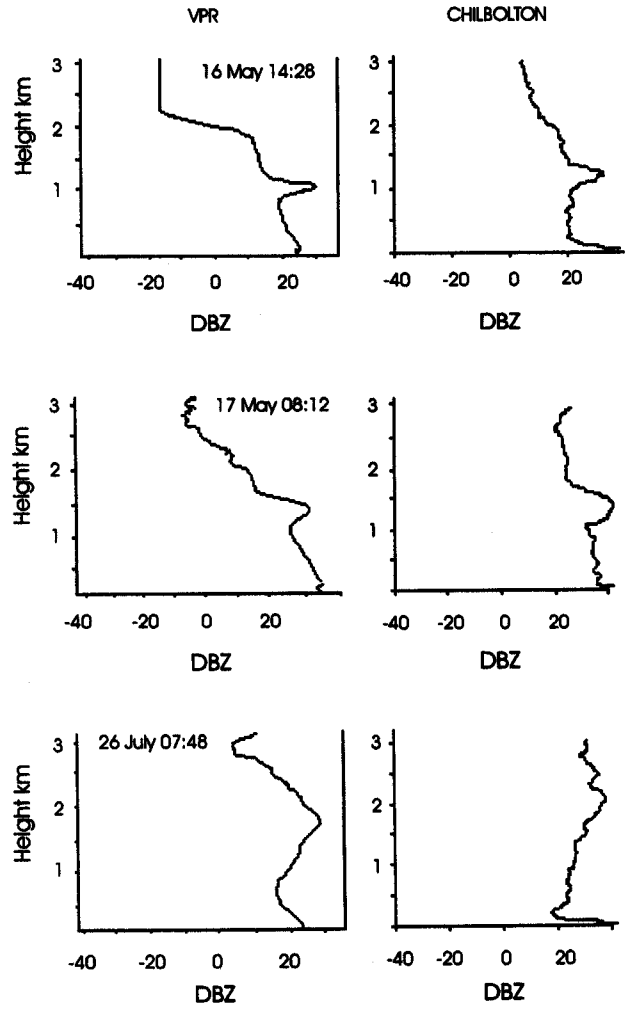

Fig. 11. *Vertical reflectivity profiles as observed at Middle Wallop.*

recalculated Z values increased to a value more in line with that actually measured by the VPR. If these new, assumed reflectivity time series are then regressed in the same manner as before, the average difference between VPR reflectivity and disdrometer reflectivity falls to a value of 4.6 dBZ. This leads to the conclusion that small point sample measurements as represented by the disdrometer (and raingauges), which are particularly prone to wind turbulence, are likely to underestimate rainfall amounts for events whose DSD are dominated by small drops. This is thought to be one of the reasons for the difference between VPR measurements and disdrometer estimates of reflectivity.

A COMPARISON OF CHILBOLTON AND VPR Z_{VP} DATA

Vertical profiles of reflectivity at the Middle Wallop site were constructed from the Chilbolton RHI data that occurred nearest to a vertical column directly above the VPR (at a range of 8.375 km from the Chilbolton radar). A series of profiles was constructed in this way for the events

of 16 and 17 May and 26 July, 1995. Unfortunately, no Chilbolton data were collected on the 11 May.

Since each RHI scan takes approximately seven seconds, each Chilbolton Z_{vp} (Ch Z_{vp}) was regarded as instantaneous and occurring at the time of the start of the RHI scan. VPR data, temporally averaged over five minute periods were calculated for the times corresponding to each RHI, the central time of each five minute VPR profile corresponding to the start time of the RHI scan. A temporal average of five minutes was used to provide temporal smoothing of the VPR Z_{vp} without removing important process information.

Rainfall on the 17 May lasted for approximately 2 hours and was of high intensity with some rainfall rate measurements exceeding 20 mm hr^{-1} with event accumulations between 6 and 8 mm. Rainfall on the 26 July was associated with thunderstorms that affected south west England throughout the morning. A series of intense precipitation cells passed the Middle Wallop site between 06.00 and 09.00, generating rainfall intensities exceeding 20 mm hr^{-1}. Unfortunately, disdrometer data was intermittent on the 17 May because of an electrical fault and another power failure on the 26 July makes disdrometer and VPR comparisons difficult.

Figure 10 compares Ch Z_{vp} and VPR Z_{vp} data for the three case study events. The shape of the vertical profile and, in particular, the height and depth of the bright band

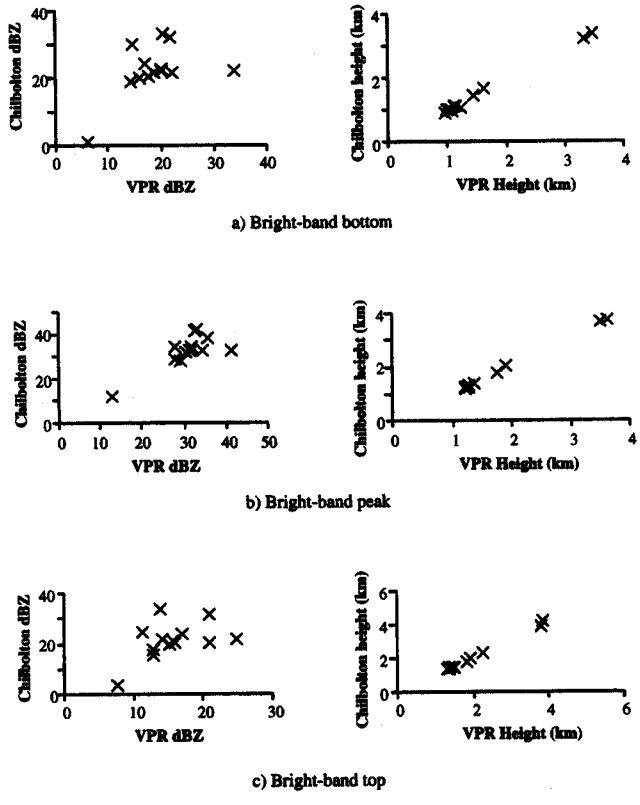

Fig. 12. *Scattergrams of principal bright band characteristics identified from VPR and Chilbolton radar data.*

are in close agreement. The primary bright band characteristics of height and reflectivity of the top, bottom and peak were identified objectively using an Automatic Bright Band Recognition Algorithm (ABBRA) developed by Tilford *et al.* (1995) for use with VPR Z_{vp} data and extended for use with the Ch Z_{vp} data. This enabled a direct objective comparison between the Ch Z_{vp} and VPR Z_{vp} data. ABBRA finds the bright band from a vertical profile by first smoothing the profile and then inspecting the rate of change of reflectivity with height. The maximum in the rate of change of reflectivity with height is sought, searching from the lowest levels upwards. A corresponding minimum is then sought above this level. These two heights are recorded, as are the reflectivity values below and above the bright band and the maximum bright band reflectivity. The data were smoothed in time using a running average filter, to give values of a nominal time resolution of 1 minute. This approach of using slope to identify the depth of the bright band is similar to that of Fabry (1994).

A simple linear regression analysis was conducted to quantify the relationship between the principal bright band characteristics as observed by the VPR and Chilbolton. The scattergrams are shown in Fig. 12. The bright band top, bottom and peak height data are in very close agreement (all r = 0.99). The least squares best fits for each gives linear relationships of the form:

$$\text{Top:} \quad y = 1.07\,x - 0.10 \tag{7}$$

$$\text{Peak:} \quad y = 1.06\,x - 0.08 \tag{8}$$

$$\text{Bottom:} \quad y = 0.98\,x - 0.02 \tag{9}$$

where, for the purposes of the regression, the VPR data were treated as the independent variable.

The small discrepancies between the two can be explained in a number of ways including different resolutions of the two devices, non-idealised beam propagation of the Chilbolton radar beam and possible attenuation of the VPR beam (which for the purposes of this study has been discounted because of the low rainfall intensities and ranges involved) as well as possible errors in the bright band recognition programme.

The actual reflectivity measurements for the bright band characteristics are poorly correlated. Overall, the VPR slightly underestimates the maximum reflectivity values compared to the Chilbolton data and the correlations between bright band top and bottom reflectivities are poor. Analysis of the data suggests underestimation by the VPR. The VPR does exhibit low-level increases in reflectivity, especially below 500 m. Return power is digitised and a $1/r^2$ range correction is applied in the software. Thus, if any errors in the dB/Volt calibration of the receiver exist, they are range corrected as well. These errors are particularly dominant below 1 km and the observed low-level enhancement is more a product of this than of any physical enhancement.

Bright band studies

Variability in the Z_{vp} due to rainfall drift and growth and/or evaporation of rainfall can render a scanning radar beam aloft unrepresentative of rainfall at or close to the surface. The most significant of these potential error sources, particularly in mid-latitudes is the presence of a bright band which can result in rainfall intensities being overestimated by up to a factor of ten (Collier, 1986a, b: Tilford, 1992). A detailed analysis of high resolution Z_{vp} data has been used to extend understanding of bright band characteristics and support the development of numerical models for correcting errors in quantitative precipitation estimates derived from scanning weather radars.

Several studies have been conducted since installation of the first VPR at Salford in April, 1991. These have included analysis of the long term database of bright band climatology as well as an initial assessment of the spatial variability of the bright band height in conjunction with data from the Chilbolton radar.

BRIGHT BAND STATISTICS OVER MANCHESTER

ABBRA was used to derive the principal bright band parameters (height and reflectivity of bright band top, bottom and peak; enhancement of bright band peak over reflectivity 100 m below the bright band) from a three year database of VPR data (Towers, 1996).

The results of an analysis of bright band heights (Fig. 13) reveal a bimodal distribution with two maxima at approximately 650 m and 1850 m. The probability curve shows that more than 30% of measured bright band occurrences are at or below 1000 m with a maximum observed height of 3800 m. Seasonal distributions of peak height were also found in the data with 60% of bright bands occurring at or below 1000 m during the period December to February and 30% at or below 1000 m during autumn and spring. These represent a significant problem when considering contamination of scanning weather radar data.

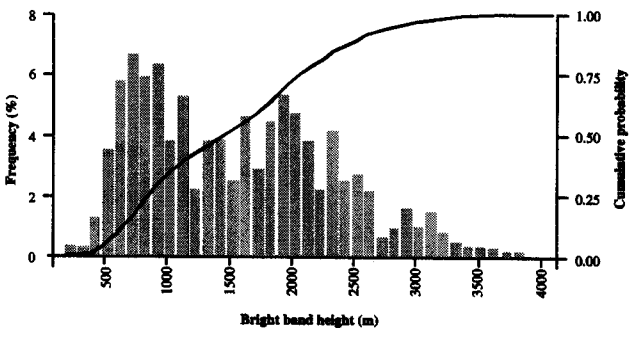

Fig. 13. *Frequency analysis of long term bright band statistics for the Salford dataset.*

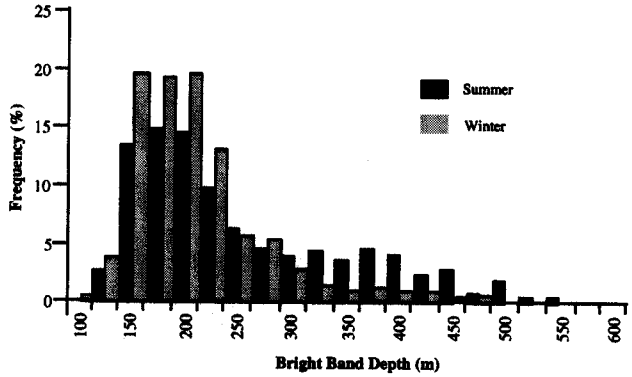

Fig. 14. *Frequency analysis of bright band depth during winter and summer for the Salford VPR dataset.*

Figure 14 shows the vertical depths of bright bands observed at Salford for summer and winter. Average depths for the two seasons are 244 m and 199 m respectively with a mean depth for the entire data set of 207 m and a maximum recorded depth of 600 m. The slightly higher summer mean and greater spread of values may indicate a very weak seasonality, but this is not statistically significant. However, these figures depend on the delineation technique used to define the bright band top and bottom heights. These results agree closely with the results from a similar study conducted in Montreal by Fabry and Zawadski (1995).

The enhancement of the bright band is defined arbitrarily as the reflectivity of the bright band peak minus the reflectivity 100 m below the bright band bottom. Using this definition, an average enhancement of 5.6 dBZ and a maximum enhancement of 11.5 dBZ were derived. The average value was derived over a range of rainfall intensities; in terms of the magnitude of the errors introduced into scanning radar estimates of surface rainfall rates, it will be progressively more critical at high rainfall rates.

During this study, the rainfall systems were classified very broadly according to whether they were stratiform or convective. Stable cloud forms are typically called stratiform clouds which characteristically have wide horizontal extents compared with their depths, diffuse outlines and weak vertical air motions which are forced either dynamically by turbulence or by topography. Formation is usually a result of advection (movement) of a moist airmass over a cool surface under stable atmospheric conditions. Convective clouds develop in conditions of atmospheric instability through the formation of rising thermals or through the release of potential instability, triggered for example by forced ascent over topography.

Of the rainfall events studied, 48% were classified as true stratiform (widespread rainfall with a bright band and more or less uniform reflectivity in the rain region) and 34% mixed stratiform and convective (widespread rainfall with a bright band and more intense embedded cells). Therefore, 82% of the events studied contained a bright band. The monthly distributions of bright band frequency indicate that

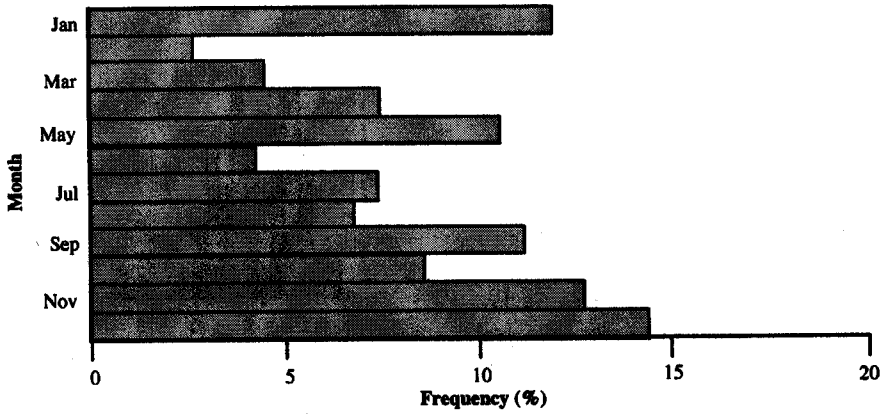

Fig. 15. *Frequency distribution of bright band occurrence by month as identified from the Salford VPR data archive.*

they are most likely during the period September through to January (Fig. 15).

SPATIAL VARIABILITY OF THE BRIGHT BAND

An initial assessment of the variability of bright band height in the Hyrex study region has been conducted using measurements of the bright band within Chilbolton RHI data for three events 16 and 17 May, and 26 July, 1995 (33, 6 and 20 RHI respectively). Estimation of the principal bright band parameters as described earlier for the three events has been conducted to obtain bright band height information with range using Middle Wallop as a reference site. The VPR bright band parameters are then used as a reference to assess bright band spatial variability.

A simple positive or negative deviation of the bright band peak reflectivity height per kilometre is used to provide a measure of the change in height with range from Middle Wallop. The results of the average deviation with range (of all the RHI data sets) are depicted in Fig. 16. The analysis was limited to a range of 50 km from the Chilbolton radar to ensure that the vertical resolution of the radar data was sufficient for the ABBRA procedure to delineate the bright band accurately.

Rainfall on the 16 May was generated above the bright band. An unstable layer existed immediately above the freezing level which contributed to outbreaks of convection in the snow layer. The rainfall was widespread and of moderate intensity and these conditions persisted during the event. Figure 16a shows little bright band height deviation from the reference height at Middle Wallop.

Much of the deviation in bright band height from the reference height for the 17 May (Fig. 16b) can be attributed to a poorly defined bright band in the RHI data which can be seen in the rapid fluctuation of the heights. The convective characteristic of the rainfall, which manifests itself as strong reflectivity gradients spatially and throughout the vertical and not just at the bright band, made the discounting procedure subjective. Most of the deviations were within 200 m of the reference height.

For the 26 July event (Fig. 16c), the average difference

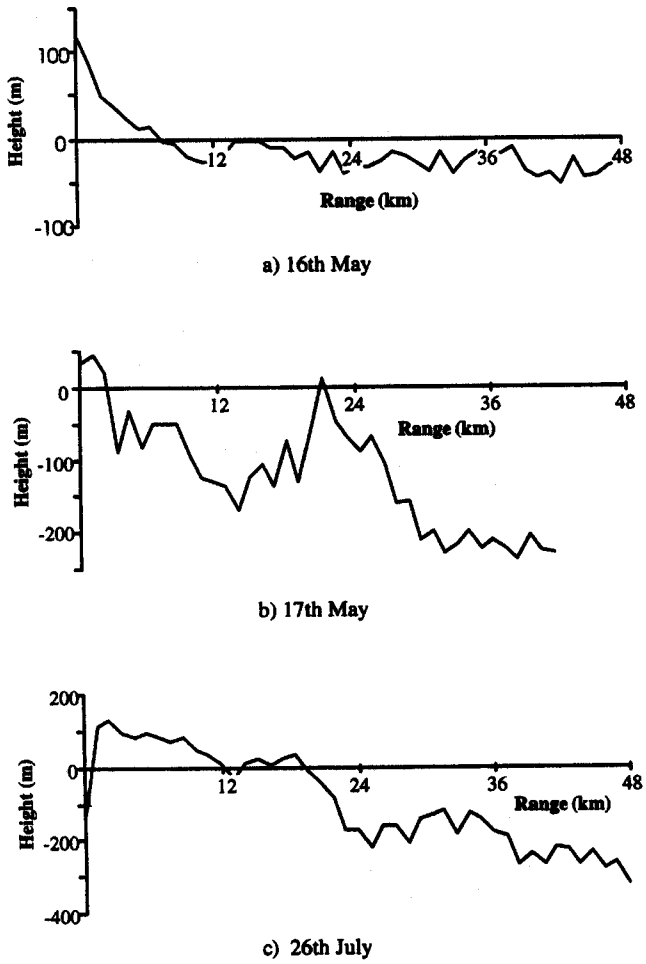

Fig. 16. *Mean height differences between bright band peak as observed by the Chilbolton radar and Middle Wallop VPR with range from Middle Wallop.*

between VPR and Chilbolton bright band height data decrease with range, probably due to the presence of a cold front to the west of Chilbolton (bright band height decreases usually being linked to a decrease in surface temperature). The rainfall on this day was characterised by scattered thunderstorms the warm updraughts and cold downdraughts of which modify the height of the 0°C isotherm height and hence the height of the bright band. This may explain the lack of dependence of bright band height on surface temperature. The resulting estimated deviations in height were up to 600 m below the reference height.

Conclusions

A VPR was built, commissioned and deployed as part of the Hyrex project. A large volume of data has been collected providing valuable information on the characteristics and dynamism of the vertical reflectivity profile across a range of temporal scales. Two mobile units were located initially at sites close to the Chilbolton radar to intercompare the vertical reflectivity profile as measured by the radars. Increased understanding of the radar-based observation techniques and bright band climatology and characteristics in the UK has been made.

Comparisons of VPR rainfall reflectivity measurements with surface disdrometer data validated against co-located rain gauges has revealed systematic overestimation of reflectivities by the VPR. A possible reason for this discrepancy is the small sample volume of the disdrometer and the sensitivity of the device which is believed to cause underestimation of large and small drops respectively. Gamma distributions with values of -2, 0 (the Marshall-Palmer exponential distribution) and 2 were fitted to each one minute drop size distribution measured by the disdrometer. The value of m was chosen in each case to provide a best fit to the measurements whilst taking into account the possibility of a sampling bias. Reflectivity was then recalculated using the derived values of m and measured rainfall.

An automatic procedure for identifying the bright band from vertical reflectivity profiles was applied to three events to facilitate an objective comparison of bright band characteristics using VPR and Chilbolton data. Bright band height values were highly correlated but, overall, absolute reflectivity values showed the VPR to give lower values than Chilbolton. Different wavelengths, sample volumes and orientation of the incident energy on scattering hydrometeors may account for some of the differences. Although a potential source of error, signal attenuation was not considered to be significant at the low rainfall intensities and short ranges considered: also, on occasions VPR bright band peak reflectivities were higher than Chilbolton.

Bright band statistics for Manchester from an analysis of a three year VPR database revealed the mean bright band depth to be 207 m and mean bright band enhancement to be 5.6 dBZ. Maximum values of bright band depth and enhancement were 600 m and 11.5 dBZ respectively. Of the rainfall events analysed, a bright band was present in 82% of cases of which approximately half had a bright band below 1000 m, which would cause contamination of a large proportion of data from the base beam elevation of operational scanning radars.

A preliminary analysis of bright band height variation with range showed that in an event exhibiting relatively unstable conditions immediately above the bright band, the deviation of the bright band height over 42 km was very little (less than 100 m). A second event exhibiting convection in the lowest 3 km of a neutrally stable atmosphere again showed little deviation over the same range (within 200 m). A third event exhibiting thunderstorm conditions showed the greatest deviation of up to 600 m over the same range; this is to be expected in conditions of significant convection.

The VPR has provided detailed numerical information on the vertical reflectivity profile. Although comparisons of VPR measurements with independent measurements at ground level and aloft reveal some discrepancies in observed reflectivity, much can be explained by the different sampling methods of each of the devices. Considerable potential exists for the development of a real-time correction scheme for scanning radars using either measurements or a parameterised version of the vertical reflectivity profile based on measurements. The improved reliability and estimation of quantitative areal precipitation as a consequence of the implementation of such a technique will be beneficial to all end users of radar rainfall data.

Acknowledgements

The authors would like to express their thanks to the following individuals and organisations without whose co-operation this research could not have been undertaken: NERC funded the project under Grant GST/02/712; North West Water Ltd. gave additional financial contributions towards the construction of the mobile VPRs; the Environment Agency; Mr. J. Goddard of the Rutherford Appleton Laboratory; Squadron Leader L. Sullivan, Boscombe Down Airfield; and Mr. T. Shaw, PSA Office, Army Air Corps Centre, Middle Wallop.

References

Andrieu, H. and Creutin, J.D., 1995. Identification of vertical profiles of reflectivity for hydrological applications using an inverse method. Part II: sensitivity analysis and case study. *J. Appl. Meteorol.*, 34, 240–259.

Austin, P.M. and Bemis, A.C., 1950. A quantitative study of the bright band in radar precipitation echoes. *J. Meteorol.*, 7, 145–151.

Battan, L.J., 1973. *Radar observations of the atmosphere*. University of Chicago Press. 324 pp.

Battan, L.J. and Bohren, C.F., 1982. Radar backscattering by melting snowflakes. *J. Appl. Meteorol.*, **21**, 1937–1938.

Bringi, V.N. and Chandrasekar, V., 1987. Simulation of radar reflectivity and surface measurements of rainfall. *J. Atmos. Ocean Tech.*, **4**, 464–479.

Byers, H.R. and Coons, R.D., 1947. The bright line in radar cloud echoes and its probable explanation. *J. Meteorol.*, **4**, 75–81.

Carbone, R.E. and Bohne, A.R., 1975. Cellular Snow Generation–A Doppler Radar Study. *J. Atmos. Sci.*, **32**, 1384–1394.

Collier, C.G., 1986a. Accuracy of Rainfall Estimates by Radar, Part 1: Calibration by Telemetering Raingauges. *J. Hydrol.*, **83**, 207–223.

Collier, C.G., 1986b. Accuracy of Rainfall Estimates by Radar, Part 2: Comparison with Raingauge Network. *J. Hydrol.*, **83**, 225–235.

Cunningham, R.M., 1947. A different explanation of the bright line. *J. Meteorol.*, **4**, 163.

Fabry, F., 1994. *Observations and uses of high resolution radar data from precipitation.* Ph.D. thesis, McGill University, Montreal, Canada.

Fabry, F. and Zawadski, I., 1995. Long Term Radar Observations of the Melting Layer of Precipitation and their Interpretations. *J. Atmos. Sci.*, **52**, 838–851.

Goddard, J.W.F., Eastment, J.D. and Thurai, M., 1994. The Chilbolton Advanced Meteorological Radar: a Tool for Multi-disciplinary Atmospheric Research. *J. Electron. Communication Eng.*, April, 77–86.

Gray, W.R. and Uddstrom, M.J., 1997. The horizontal variability of the vertical profile of reflectivity. *Amer. Meterol. Soc., 28th international radar conference*, Austin, Texas, USA, 8th–12th September.

Gray, W.R., 1991. *The vertical profile of reflectivity and errors in radar estimates of rainfall.* Ph.D. Thesis, University of Reading, UK, 202 pp.

Hardaker, P.J., 1993. *A study of the melting layer in single polarisation radar echoes with application to operational weather radar.* Ph.D. thesis, University of Essex, UK.

Hardaker, P.J., Holt, A.R. and Collier, C.G., 1995. A melting layer model and its use in correcting for the bright band in single polarisation radar echoes. *Quart. J. Roy. Meteorol. Soc.*, **121**, 495–525.

Harrold, T.W. and Kitchinman, P.G., 1975. Measurement of surface rainfall using radar where the beam intersects the melting layer. *Proceedings of the 16th Conference on Radar Meteorology, Amer. Meteorol. Soc.*, 473–478.

Herman, B.M., Browning, S.R. and Battan, L.J., 1961. *Tables of the radar cross sections of water spheres.* Technical Report 9, Tucson, Institute of Atmospheric Physics, University of Arizona.

Hobbs, P.V. and Locatelli, J.D., 1978. Rainbands, Precipitation Cores and Generating Cells in a Cyclonic Storm. *J. Atmos. Sci.*, 35, 230–241.

Houze, R.A., Hobbs, P.V., Herzegh, P.H. and Parsons, D.B., 1979. Size distributions of precipitation particles in frontal clouds. *J. Atmos. Sci.*, **36**, 156–162.

Illingworth, A.J., Blackman, T.M. and Goddard, J.W.F., 2000. Improved rainfall estimates in convective storms using polarisation diversity radar. *Hydrol. Earth Syst. Sci.*, **4**, 555–563.

Joss, J. and Waldvogel, A., 1970. *Distrometer RD-69. Instruction Manual*, Distromet Ltd., PO Box 33 CH-4020 Basel, Switzerland, 32 pp.

Joss, J. and Waldvogel, A., 1990. Precipitation measurement and hydrology. Battan memorial and radar conference. Ed. D. Atlas, *Amer. Meteorol. Soc.*, 577–606.

Kitchen, M., Brown, R. and Davies, A.G., 1994. Real-time correction of weather radar data for the effects of bright band, range and orographic growth in widespread precipitation, *Quart. J. Roy. Meteorol. Soc.*, **120**, 1231–1254.

Klaasen, W., 1988. Radar observations and simulation of the melting layer of precipitation. *J. Atmos. Sci.*, **45**, 3741–3753.

Koistinen, J., 1992. Operational correction of radar precipitation errors due to the vertical reflectivity profile. *2nd International Symposium on the Hydrological Applications of Weather Radar*, University of Hannover, September 7–10th.

Lhermitte, R.M. and Atlas, D., 1963. Doppler fall speed and particle growth in stratiform precipitation. *Proceedings of the 10th Weather Radar Conference, Amer. Meteorol. Soc.*, 297–302.

Marshall, J.S., 1953. Precipitation Trajectories and Patterns. *J. Meteorol.*, **10**, 25–29.

Marshall, J.S. and Palmer, W.M.K., 1948. The Distribution of Raindrops with Size. *J. Meteorol.*, 5, 165–166.

Moore, R.J., Jones, D.A., Cox, D.R. and Isham, V.S., 2000. Design of the HYREX raingauge network. *Hydrol. Earth Syst. Sci.*, **4**, 523-530.

Plank, V.G., Atlas, D. and Paulson, W.H., 1955. The Nature and Detectability of Clouds and Precipitation as Determined by a 1.25 cm Radar. *J. Meteorol.*, **12**, 358–377.

Rogers, R.R. and Yau, M.K., 1989. *A short course in cloud physics.* Pergamon Press, 293 pp.

Sempere Torres, D., Porra, J.M. and Creutin, J.D., 1994. A general formulation for rain drop size distribution. *J. Appl. Meteorol.*, **33**, 1494–1502.

Smith, C.J., 1986. The reduction of errors caused by bright bands in quantitative rainfall measurements made using radar. *J. Atmos. Ocean Tech.*, **3**, 129–141.

Steiner, M. and Waldvogel, A., 1989. The bright band and its influence on microphysics. *Proceedings of the 24th Int. Conference on Radar Meteorology, Amer Meteorol. Soc.*, 5–8.

Stewart, R.E., Marwitz, J.D. and Pace, J.C., 1984. Characteristics through the melting layer of stratiform clouds. *J. Atmos. Sci.*, **41**, 3227–3237.

Stow, C.D., 1993. *Hydra Sensor Manual.* Internal Report of the Dept. of Physics, University of Auckland, New Zealand, 12 pp.

Tilford, K.A., 1992. *Weather radar data for operational hydrology*, PhD Thesis, Department of Civil Engineering, University of Salford, UK.

Tilford, K.A., Cluckie, I.D., Wild, A., Towers, S.Y. and Lane, A., 1994. *Local Real Time Adjustment Techniques.* Vertically Pointing Radar Project, Interim Report No. 6-Q3-93, Water Resources Research Group, Telford Research Institute, University of Salford, UK. 45 pp.

Tilford, K.A., Han, D. and Cluckie, I.D., 1995. Vertically Pointing and Urban Weather Radars. In: *Hydrological Uses of Weather Radar.* K.A. Tilford, (Ed.) British Hydrological Society Occasional Paper No. 5, 147–164. ISBN 0948540640.

Toit du, P.S., 1967. Doppler radar observations of drop sizes in continuous rain. *J. Appl. Meteorol.*, **6**, 1082–1087.

Towers, S.Y., 1996. *Vertical Reflectivity Profiles and the Correction of Operational Radar Rainfall Data.* Ph.D. Thesis, University of Salford, UK. 263 pp.

Ulbrich, C.W., 1983. Natural Variations in the Analytic Form of the Raindrop Size Distribution. *J. Climate Appl. Meteorol.*, **22**, 1764–1775.

Wexler, R. and Atlas, D., 1963. Radar reflectivity and attenuation of rain. *J. Appl. Meteorol.*, **2**, 276–280.

Willis, P.T. and Heymsfield, A.J., 1989. Structure of the melting layer in mesoscale convective system stratiform precipitation. *J. Atmos. Sci.*, **46**, 2008–2025.

Zawadski, I., Monteiro, E. and Fabry, F., 1994. The development of drop size distributions in light rain. *J. Atmos. Sci.*, **51**, 1100–1113.